

# On the Origin of Gap States in Molecular Semiconductors— A Combined UPS, AFM, and X-ray Diffraction Study

Jan Hagenlocher, Niels Scheffczyk, Katharina Broch, Giuliano Duva, Nadine Rußegger, Lisa Egenberger, Rupak Banerjee, Satoshi Kera, Frank Schreiber, and Alexander Hinderhofer\*

Cite This: *J. Phys. Chem. C* 2021, 125, 17929–17938

Read Online

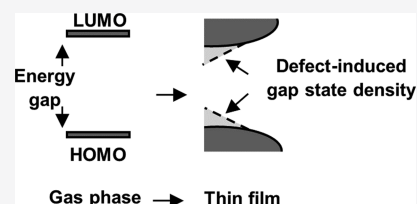
ACCESS |

Metrics & More

Article Recommendations

Supporting Information

**ABSTRACT:** Electronic states within the HOMO–LUMO gap of organic semiconductors play a key role in the energy level alignment of substrate–organic and organic–organic interfaces and therefore are a defining parameter for device functionality and efficiency. They are thought to result from structural defects influencing the specific environment of a molecule. Varying the substrate temperature for samples grown by molecular beam deposition, we are able to control their density. Using atomic force microscopy and X-ray scattering techniques, we can differentiate defects depending on their length scale and effective direction. Comparison of the respective defect density with the density of gap states, measured directly via ultra-low-background ultraviolet photoelectron spectroscopy, enables to correlate structural and electronic properties for different prototypical organic semiconductors. We investigate the impact of gap states on the energy level alignment and find a direct link between structural defects and the interface dipole.



## INTRODUCTION

The vast majority of (opto-)electronic devices based on organic semiconductors features an architecture with at least

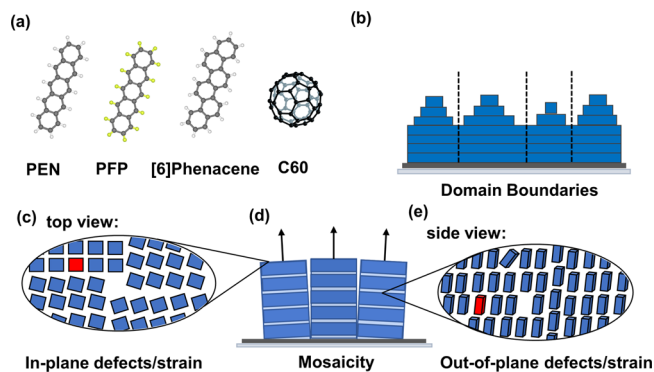


**Figure 1.** (a) Schematics of the investigated compounds: pentacene (PEN,  $C_{22}H_{14}$ ), perfluoropentacene (PFP,  $C_{22}F_{14}$ ), [6]phenacene ( $C_{26}H_{16}$ ), and C60. (b–e) Schematic representation of the different structural defects which are a possible cause of the electronic gap states, each of which represents a different length scale or orientation. Rather large defect sources such as boundaries between different domains (b) or the tilt of crystallites relative to the surface normal (d) can be distinguished from microscopic irregularities introduced by crystallite size, misfits, vacancies, or impurities [red block, (c,d)] in the in-plane and out-of-plane directions.

two different compounds forming a heterojunction.<sup>1,2</sup> Generally, this allows a precise control of device functionality and performance. Depending on the desired properties, the compounds can be mixed at the molecular level (A/B)

resulting in a blend or form a planar heterojunction (A-on-B) with an ideally sharp interface between the two organic thin films.<sup>3–5</sup> A phenomenon observed for the flat interface is the so-called energy level alignment (ELA), where the relative positions of the molecular frontier orbitals can be shifted, and energy barriers can be smaller or larger than what is theoretically expected.<sup>6–9</sup> Different mechanisms have been proposed to explain this behavior, but, until now, a unifying model is still elusive and depending on the reactivity of the substrate, different cases must be distinguished.<sup>9–14</sup> For the case of weakly interacting, inert surfaces, it was proposed that ELA is in fact governed by a small density of electronic states within the energy gap of the organic compounds (gap states).<sup>15–18</sup> They are thought to result from structural or chemical defects acting as dopants, and also, theoretical studies modelling the presence of gap states underline the importance and impact on the ELA mechanism.<sup>19–21</sup> It was demonstrated that their appearance is a common feature in molecular thin films and their density can be controlled by changing preparation parameters.<sup>15,22–25</sup> Until now, this was mainly done by chemical or molecular doping using different organic or inorganic dopants.<sup>22,26,27</sup> In the present study, an approach alternative to doping is applied: by using different substrate temperatures during the growth of the respective organic thin

Received: April 6, 2021  
Revised: July 22, 2021  
Published: August 6, 2021



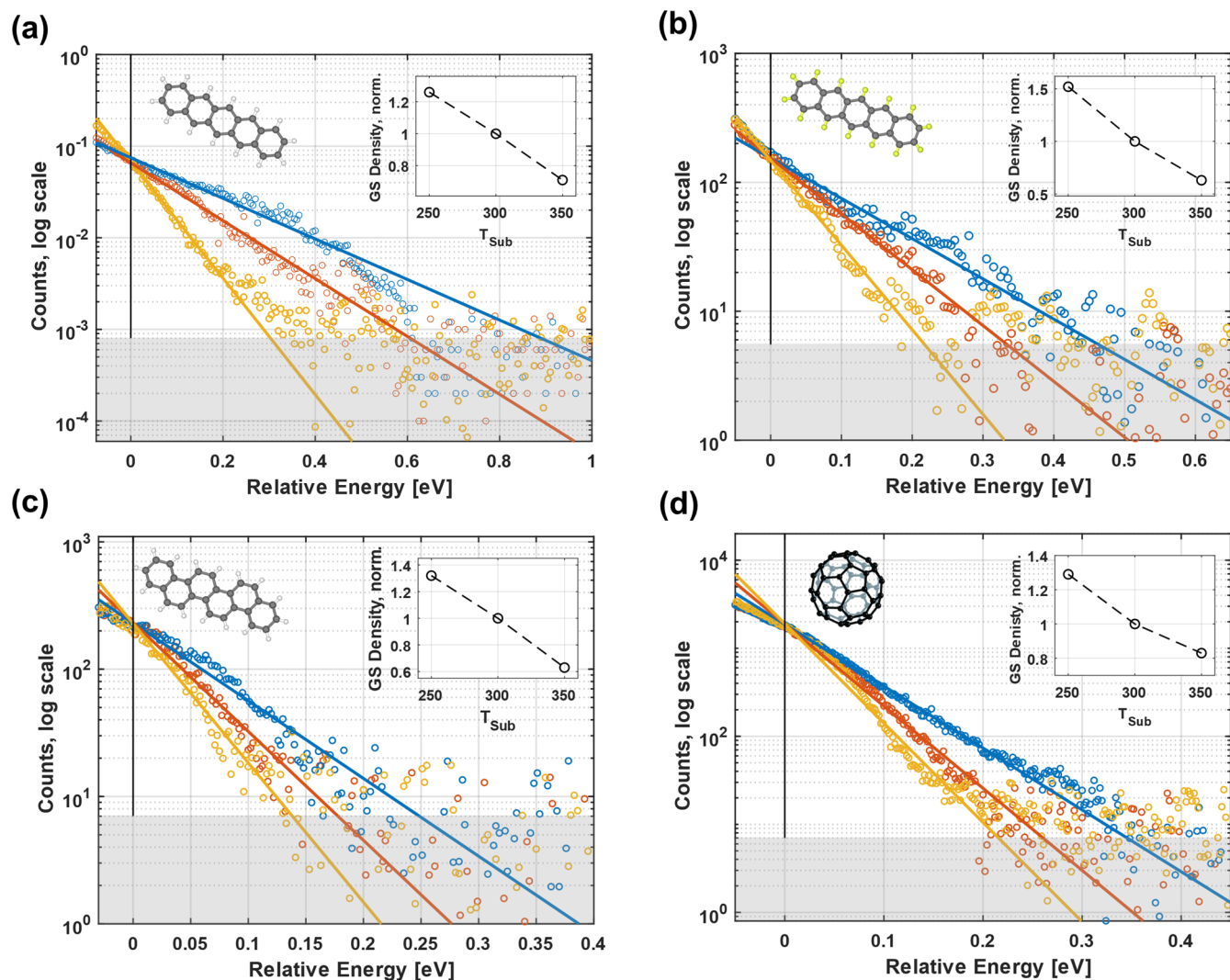


**Figure 2.** Ultra-low-background UPS spectra of the gap state region for (a) PEN, (b) PFP, (c) [6]phenacene, and (d) C60. Colors correspond to the substrate temperature during growth: blue (250 K), red (300 K), and yellow (350 K). The spectra are shifted horizontally to the respective HOMO edges to allow for a better comparison. The straight lines approximate the observed gap state densities occurring as exponential tails reaching into the band gap. The insets show the relative amount of gap states normalized to the respective room-temperature sample (300 K, red).

films, the density of structural defects can be controlled.<sup>28–30</sup> Since the ultraviolet photoelectron spectroscopy (UPS) signal of the gap states is some orders of magnitude smaller than the typical signal of valence states, a direct measurement turns out to be difficult and is only achievable by acquiring UPS data with an ultralow background. Such an approach allows for data acquisition and quantitative visualization of the density of gap states even on a logarithmic scale. Additionally, complications intrinsic in electrical transport measurements, like the effect of external contact interfaces,<sup>31,32</sup> can be overcome. We combine UPS measurements with different techniques for structural investigation to identify which kind of defect<sup>33–35</sup> is the main source of the gap states.

Our main focus lies thereby on rather large-scale domain boundaries<sup>36</sup> (Figure 1b) and microscopic dislocations, point defects, or impurities (red block) within the organic crystal,<sup>37,38</sup> which, in turn, can be divided into in-plane and out-of-plane defects (Figure 1c,e). By changing the substrate temperature during growth of the different thin films, with all other growth parameters kept constant, we are able to effectively control the density of defects.<sup>39</sup> However, due to

the dynamic nature of thin-film growth, it is quite difficult to control the density of only one specific kind of defect while keeping the others constant. For this reason, we conducted a comprehensive comparative study of four different compounds (Figure 1a) grown on a SiO<sub>2</sub> substrate and examined their respective gap state densities against the density of defects described above.

## METHODS

The samples were prepared within the UPS setup, and the gap state density was measured without breaking the vacuum ( $p < 1 \times 10^{-8}$  mbar). Before installation, the silicon substrates (ntvSi) with a native oxide layer of 2.0 nm were cleaned in an ultrasonic bath with acetone, 2-propanol, and demineralized water successively. Before each sample preparation, the substrates were heated to over 700 K overnight to desorb residues. The deposition rates were kept at 2 Å/min, which was monitored using a water-cooled quartz crystal microbalance (QCM) during growth. The molecules were evaporated from thermally shielded Knudsen cells. The ntvSi substrates were mounted on a molybdenum sample holder

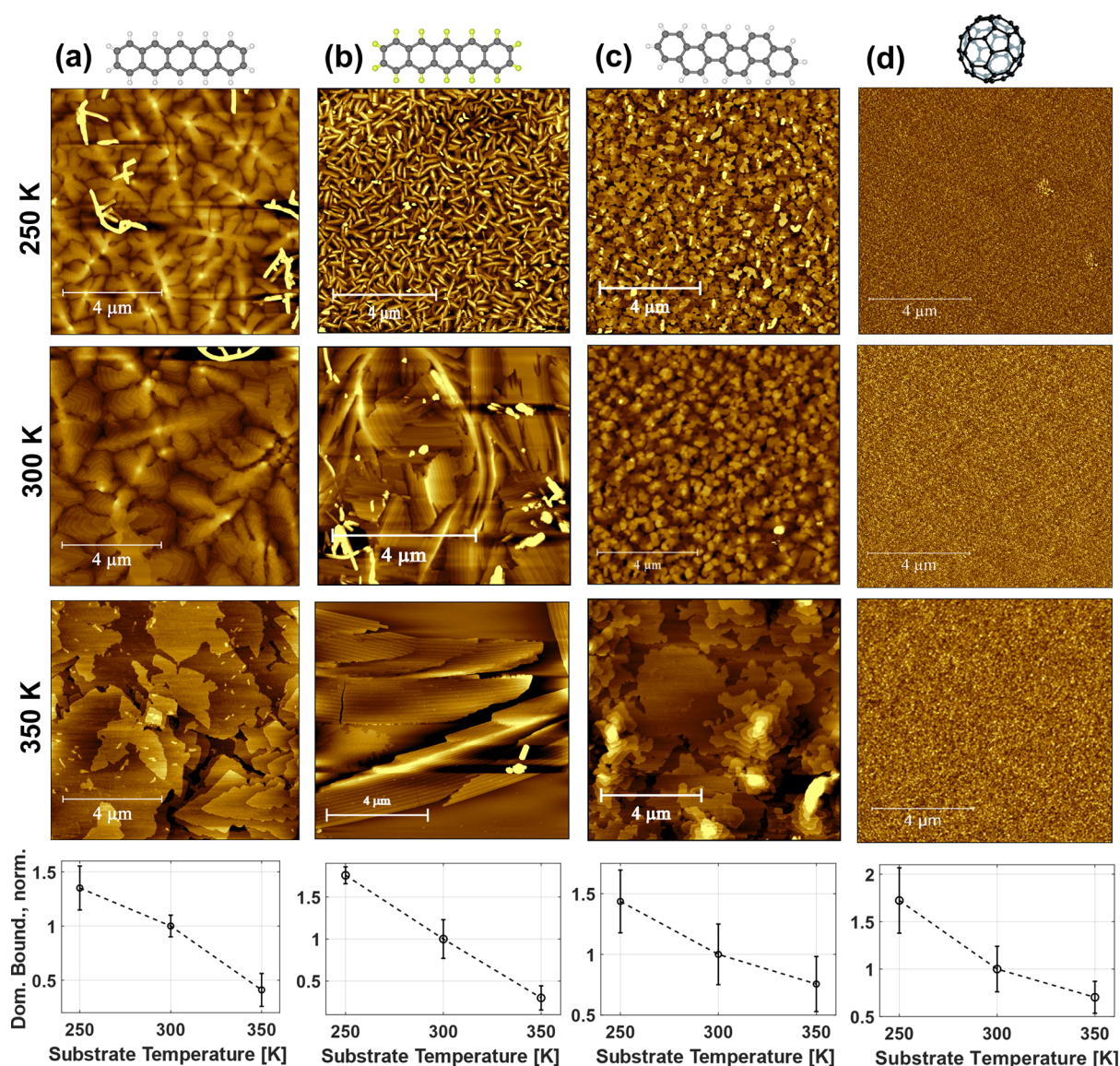


**Figure 3.** AFM images of (a) PEN, (b) PFP, (c) [6]phenacene, and (d) C60 thin films grown at 250 K (first row), 300 K (second row), and 350 K (third row), respectively. In the bottom figures, the evolution of the domain boundary length, normalized to the room-temperature sample, is shown. A general trend is the increase of domain size with the increase of substrate temperature and an accordingly decreasing domain boundary length.

with options of resistive heating and cooling by liquid nitrogen as required. The substrate temperature was monitored using a thermocouple attached to the sample holder in close proximity to the substrates. For all samples, the temperature during measurements was the same (room temperature, 300 K).

The UPS measurements were performed using an ultra-low-background, high-sensitivity UPS apparatus with a hemispherical electron analyser (MBS A-1) and either a monochromatic HeI (energy: 21.2 eV) or XeI (8.4 eV) radiation source. The gap state density spectra were typically recorded over 90 min. All UPS spectra were recorded at normal emission with an acceptance angle of  $\pm 18^\circ$ . The He or Xe light was incident at  $45^\circ$  with respect to the sample surface. A bias of  $-5$  V was applied to the sample in order to detect the secondary cutoff. PEN, [6]phenacene, and C60 were measured using a HeI discharge lamp with a photon energy of 21.2 eV and a very high surface sensitivity so that only the top few layers are probed. Only the PEN data were measured using the

XeI light source, explaining the slightly different shape  $<0$  eV due to a larger penetration depth and the measurement being more sensitive to slightly different molecular arrangements in deeper, hidden layers within the film, a common feature in PEN thin films.

The binding energy scale is referred to the Fermi level measured on a metal substrate. Ionization energy values were obtained as  $IE = E_{\text{HOMO}} + \phi = E_{\text{HOMO}} + h\nu - E_{\text{cutoff}}$  where  $\phi$  is the work function of the sample, defined as the energy separation of the vacuum level (VL) from the Fermi level.  $E_{\text{HOMO}}$  is the HOMO edge position, and  $E_{\text{cutoff}}$  is the cutoff position. Since UPS can only measure the HOMO distribution, which does not take part in the energy level alignment in the investigated systems, an increase of gap state density for the LUMO states can only be assumed. Experimentally, inverse photoelectron spectroscopy (IPES) could also be used to investigate the gap state distribution for the LUMO, but the sensitivity that can be reached is some

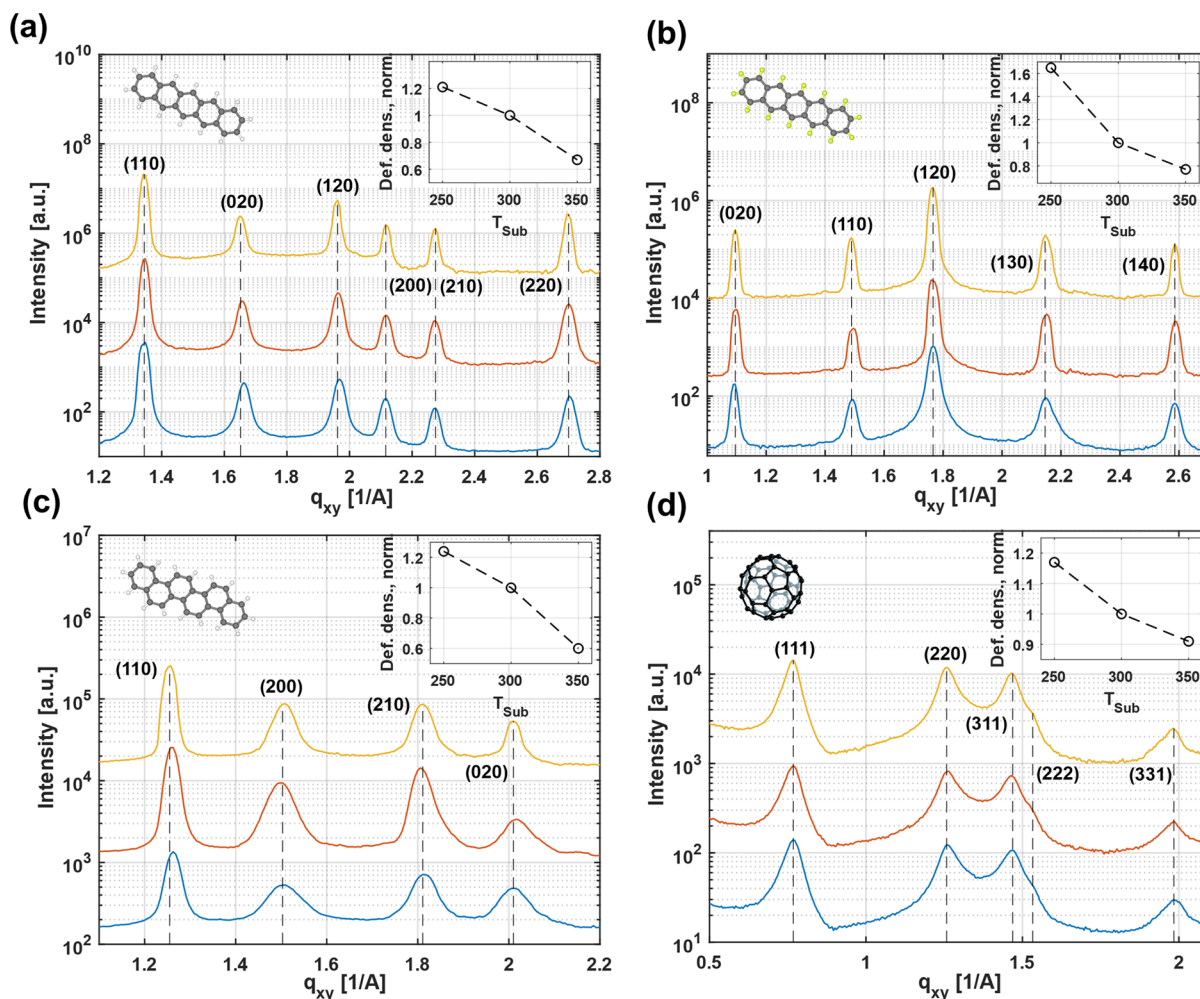


**Figure 4.** GIXD data of organic thin films: (a) PEN, (b) PFP, (c) [6]phenacene, and (d) C60. Colors correspond to the substrate temperature during growth: blue (250 K), red (300 K), and yellow (350 K). The inset shows the obtained in-plane defect density from the averaged width of the respective Bragg reflections and normalized to the room-temperature sample.

orders of magnitudes below the one for UPS, and so far, no direct detection of gap states is possible.

The X-ray experiments were done at beamline I07 of the Diamond Light Source in Didcot, U.K., and the Soleil Synchrotron in Saint-Aubin, France, using a Pilatus 100 K (Diamond) and XPAD (Soleil) detector and a monochromatic X-ray beam at 13 keV (wavelength 0.95385 Å). Slits directly in front of the detector were used to mimic a point detector where needed. An incidence angle of  $\alpha_i = 0.1^\circ$  was chosen for the grazing incidence X-ray diffraction measurements. By keeping the incoming X-ray beam at a shallow angle close to the critical angle, one obtains surface sensitive information about the arrangement of molecules in the top layers. To obtain the coherently scattering island size  $D_{coh}$ , the Bragg reflections were fitted with Gaussians functions and the full width at half-maximum (fwhm) of the  $q$ -space inserted into Scherrer's equation ( $D_{coh} = 2\pi K/\text{fwhm}$ , with  $K = 0.94$  for spherical crystallites). Rocking scans were measured by keeping the incident and exit angles of X-rays constant, which fixes the scattering vector. Rocking the sample around its central axis probes the width of a particular Bragg reflection, that is, the range for which the scattering condition is fulfilled. For the qualitative peak analysis, a reference image of a Si-

Bragg reflection was obtained. In the out-of-plane defect analysis, a contrast factor of unity was assumed.

PEN was purchased from Sigma-Aldrich with >99.9% purity, PFP (99.9% purity) was purchased from Kanto Denka Kogyo Co., [6]phenacene was bought from NARD Co., Ltd. (Japan, purity 99.9%), and C60 was bought from CreaPhys (99.9%).

## RESULTS AND DISCUSSION

**Gap State Density.** Figure 2 shows UPS data of the HOMO gap state regions of 20 nm thin films of (a) pentacene (PEN), (b) perfluoropentacene (PFP), (c) [6]phenacene, and (d) C60. For each compound, we compare three films prepared at different substrate temperatures (250, 300, and 350 K). To visualize the change in gap state density, the spectra for each compound are shifted to align with their respective HOMO edge [which corresponds to the onset in the linear scale (see Figure S1)], and the energy values are given relative to this. First, we note that for each compound, the density of electronic gap states scales with the substrate temperature. As a general feature, an increase of gap states going from the high-temperature samples (yellow) to room temperature (red) to the low-temperature samples (blue) is observed. The shape of the electronic gap states varies for different compounds and temperatures; however, it can

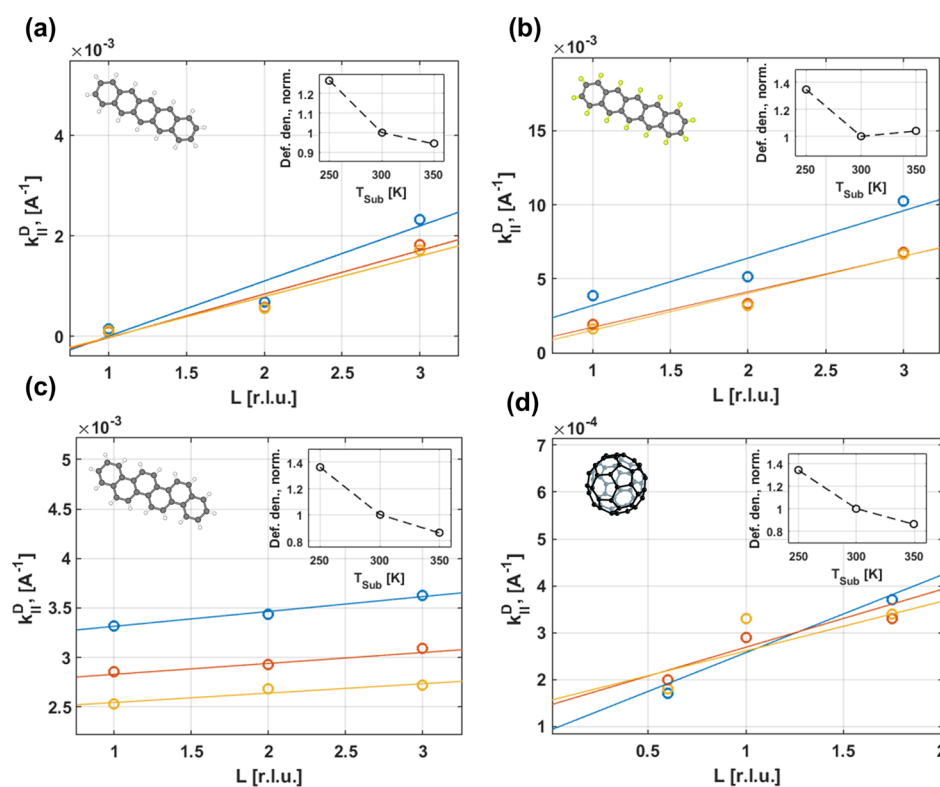


**Figure 5.** fwhm of the diffuse intensity  $k_{||}^D$  is plotted vs  $L$  (in reduced lattice units) for (a) pentacene, (b) perfluoropentacene, (c) [6]phenacene, and (d) C60. The colors correspond to the substrate temperature during growth: blue (250 K), red (300 K), and yellow (350 K). From the slope of the respective linear fits, the defect density in the out-of-plane direction can be calculated. Insets show the resulting defect density normalized to the respective room-temperature sample (red).

generally be approximated by an exponential tail, indicated by straight lines on the logarithmic scale in Figure 2. The slight deviation of the low-temperature samples of PEN and [6]phenacene could point toward the influence of a predominant type of structural defect resulting in a relatively well-defined density of additional states. For the general trend, it appears not possible to identify any specific dependency on molecular characteristics such as shape or polarity, suggesting that the phenomenon is widespread and expected to be found also in thin films of other compounds. For better comparison, the density [i.e., the integrated area below the exponential tail and above the background signal (gray rectangle)] is normalized to the area of the respective room-temperature sample and displayed in the insets. In the following, we quantify the density of different types of structural defects for the different organic molecules and correlate them to the density of electronic gap states.

**Domain Boundaries.** To determine the density of defects from large domain boundaries (Figure 1b), we measured height profiles of each sample using atomic force microscopy (AFM). The top three rows of Figure 3 show AFM data from PEN (a), PFP (b), [6]phenacene (c), and C60 (d) at the three different growth temperatures. The thin-film morphology of all compounds is strongly affected by the substrate temperature. In general, we find an increase in domain size for higher-temperature samples and, in turn, a decrease of boundary length between adjacent domains. To quantify the domain size changes, we extracted the boundary lengths using the software Gwyddion<sup>40</sup> and its built-in grain-detection function (see Figure S2) for at least three different AFM images per sample. Comparing the trend by normalizing to the room-temperature

film, as was done for the density of electronic gap states, we find the boundary length increasing between a factor of 1.75 for the low-temperature PFP sample to 1.35 for the low-temperature PEN sample, with the decrease reaching to 0.76 for high-temperature [6]phenacene to approximately a factor of 0.30 for the high-temperature PFP sample compared to the respective 300 K films (Figure 3, bottom row). Comparing the domain boundary length extracted from each of the AFM images with the density of electronic gap states (Figure 2, insets), we find that both decrease for the high-temperature samples, however with a somewhat different scaling.

**In-Plane Defects.** Using X-ray techniques allows to study structural defects also related to the crystal structure. Figure 4 shows grazing incidence X-ray diffraction (GIXD) data of organic thin films of (a) PEN, (b) PFP, (c) [6]phenacene, and (d) C60, deposited at different substrate temperatures. All samples are polycrystalline and, consistent with the literature, PEN, PFP, and [6]phenacene thin films exhibit a so-called fiber texture (2D powder) with the two short unit cell axes parallel to the substrate.<sup>41,42</sup> In contrast, C60 exhibits Bragg reflections consistent with randomly distributed domain orientations (3D powder).<sup>43</sup> In general, Bragg peak positions for different growth temperatures are rather identical for each compound, indicating that the crystal structure is not affected by a change of growth temperature. Therefore, different polymorphs can be ruled out as sources of the different gap state densities. However, analyzing the width of Bragg reflections, the in-plane coherently scattering island size  $D_{\text{coh}}$  can be obtained.  $D_{\text{coh}}$  depends mainly on strain, dislocations, and point defects (misfits, vacancies), which reduce the long-range crystalline order in the thin films<sup>44,45</sup> and can be

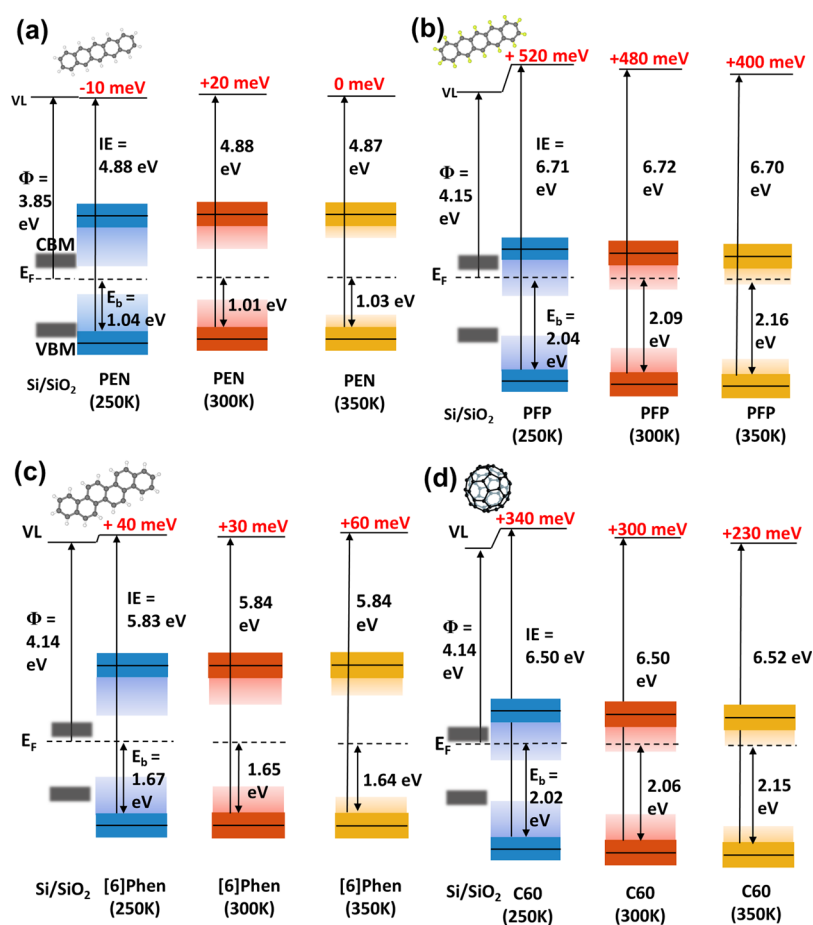


**Figure 6.** Schematic representation of the ELA of (a) PEN, (b) PFP, (c) [6]phenacene, and (d) C60. For PFP and C60, a positive ID (indicated in red), resulting from electrons moving from the substrate into the “empty” LUMO states, dependent on the gap state density can be observed. For PEN and [6]phenacene, the energy barrier between Fermi energy and both the HOMO and LUMO states is too large, leading to no transferred charges and no gap state density-dependent ID. Also indicated are the conduction band maximum (CBM) and the valence band minimum (VBM) of the substrate. We expect the electrons to be transferred from the partially filled conduction band into the empty LUMO states of the respective compound.

converted into an areal defect density via  $1/D_{\text{coh}}$ .<sup>46,47</sup> For the analysis, the width (in terms of the full width at half-maximum, fwhm) of the observed reflections for each film was determined and the resulting  $D_{\text{coh}}$  averaged. As a general trend,  $D_{\text{coh}}$  increases with elevated substrate temperatures and the defect density, which is inversely proportional to  $D_{\text{coh}}$  decreasing accordingly. Normalization to the room-temperature sample gives the variation of the defect density on the substrate temperature. Decreases to a factor of about 0.6 for the high-temperature [6]phenacene sample and 0.8 for the high-temperature PEN sample are observed. The increase of defects lies between 1.2 for the C60 sample grown at low temperature and up to 1.6 for the PFP low-temperature sample. The temperature dependence, in general, is in good accordance with the gap state density discussed above.

**Out-of-Plane Defects.** Due to dislocations and distortions, the reciprocal lattice points of a real crystal are misoriented and displaced relative to the ideal lattice, resulting in a diffuse scattering signal. Following a method introduced by Nickel et al.,<sup>37</sup> the increasing width of the diffuse scattering signal in rocking scans can be converted into a defect density. By analyzing the broadening solely in the direction of the surface normal [i.e., along (00L) reflections], we can extract the density of defects in the out-of-plane direction. Figure 5a–d

shows the dependence of the fwhm (as  $k_{\text{II}}^{\text{D}}$ , obtained from Gaussian fits of the diffuse scattering signal) on the momentum transfer  $L$ . Characteristically, we find a linear increase for which the slope can be directly converted into the defect density for an unchanging film thickness. As apparent from the normalized defect density shown in the insets, we find a strong decrease of the out-of-plane defect density when changing from low to room temperature for all investigated systems. On the other hand, a change of growth temperature from room temperature to high temperature has a much weaker impact on defect density (also compared to the other kinds of examined defects). For PFP, we even find a small increase in the number of out-of-plane defects at a higher temperature. Apart from the method described here, there are more possibilities to investigate the density of out-of-plane defects, with the Williamson–Hall analysis (WHA) being the most prevalent. The results from the WHA and the analysis of the average tilt of crystallites with respect to the surface normal (mosaicity) highlighting the same general trend are shown in the Supporting Information (Figures S3 and S4).

**Energy Level Alignment—Impact of Gap State Density.** Last, the impact of the gap state density on the interface dipole (ID) between the substrate and the organic thin film is studied. Figure 6 shows the ELA of (a) PEN, (b)

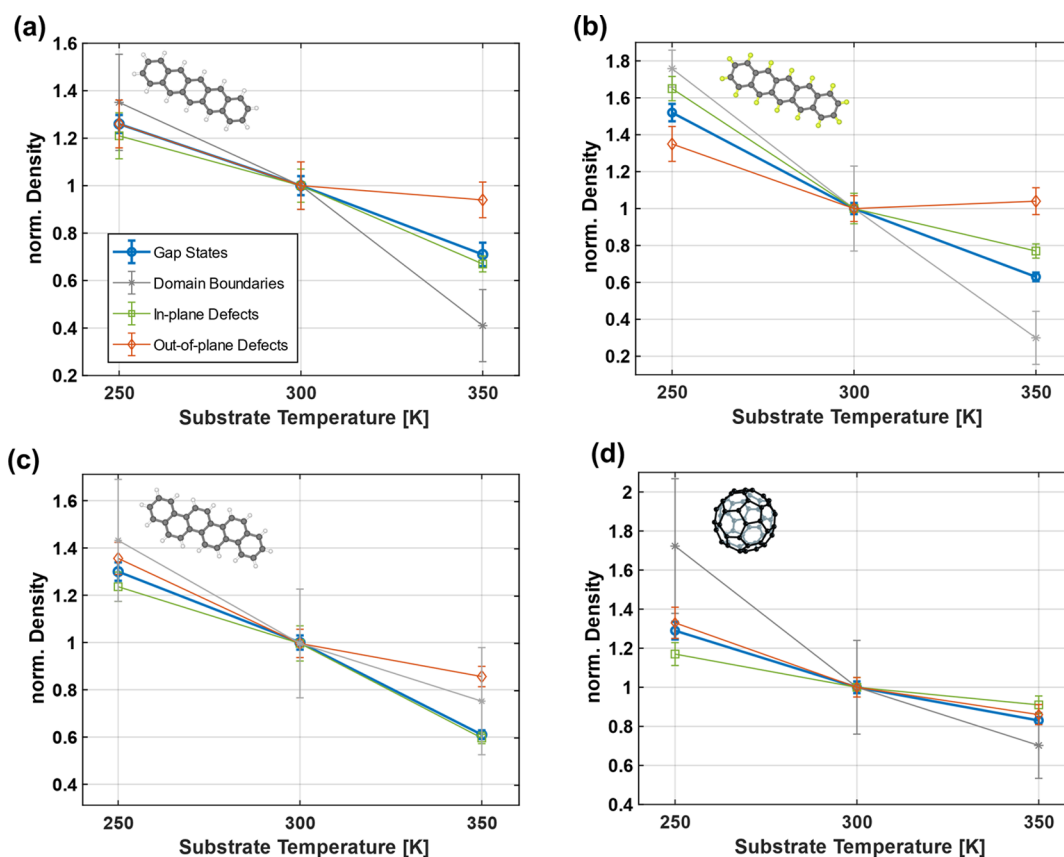


**Figure 7.** Gap state densities and structural defect densities for different organic compounds grown at different substrate temperatures.

PPF, (c) [6]phenacene, and (d) C60 on a silicon substrate. In general, within the gap state model, the ELA between the substrate and organic film is governed by the energy distance between the substrate Fermi energy and the HOMO (LUMO) distribution as well as the exact shape of the distribution.<sup>20</sup> As shown in Figure 2, the density distribution of gap states depends strongly on the substrate temperature during growth and differs for the investigated systems. For example, the extension of states may reach an additional 100 meV for low-temperature [6]phenacene and as much as 400 meV for low-temperature PFP into the electronic gap compared to the respective high-temperature sample. Here, it has to be noted that so far, due to experimental restrictions, only a direct measurement of HOMO gap states is possible. The direct detection of gap states reaching out from the LUMO level, which is principally accessible with inverse photoelectron spectroscopy (IPES), is still elusive. However, the impact of an altered LUMO gap state density on the ELA can be studied using a conventional UPS setup and is evident from the PFP and C60 data, where a positive interface dipole (ID, indicated in red) can be observed. This can be attributed to a charge transfer through tunneling from the substrate into the empty LUMO gap states of the organic layer.<sup>20,48</sup> Since the substrate work function was identical for most of the compounds, a change in magnitude in the ID can be exclusively ascribed to the broadening of the LUMO distribution (i.e., gap state density). With more gap states accessible, more electrons can be transferred, thus leading to a higher observed ID. For PEN and [6]phenacene, the energy barrier between Fermi energy and both the HOMO and LUMO states is too large, leading to no transferred charges, and no gap state density-dependent ID

can be observed. The LUMO positions (electron affinities, EA) indicated here are taken from IPES measurements found in the literature:  $EA_{PEN} = 2.35$  eV,<sup>49</sup>  $EA_{PPF} = 4.12$  eV,<sup>49</sup>  $EA_{C60} = 3.98$  eV.<sup>50</sup> For [6]phenacene, no IPES data can be found. However, the electron affinities of the closely related [5]- and [7]phenacenes are 3.2 eV<sup>51</sup> for [5]phenacene and 3.1 eV<sup>51</sup> for [7]phenacene. Assuming a linear dependence of the energy gap width as for acenes, we estimate EA of [6]phenacene to be 3.15 eV.

## CONCLUSIONS

We investigated the impact of different structural defects on the gap state density of four prototypical organic semiconductors as well as the role of such defects in the ELA by complementary X-ray scattering, AFM, and ultra-low-background UPS measurements. Varying the growth temperature of the respective thin films allows us to control the density of electronic gap states, with a lower temperature leading to a higher density of observable states. Comparing the dependence of gap states and structural defect density on growth temperature, we can link the two aspects and even pinpoint the impact of defects of different spatial distributions and length scales. In Figure 7, the gap state density and the different defect densities are summarized. In general, the density of all types of defects decreases with a higher substrate temperature; however, the exact temperature dependence is somewhat different. Notably, the in-plane defect density obtained from the coherently scattering size  $D_{coh}$  is in good agreement with the gap state density variation. Since gap states are thought to result from deviations in the overlap of molecular orbitals and the rod-like compounds grow standing

up and in a layered fashion, the overlap is mainly localized inside planes parallel to the substrate. A smaller (in-plane)  $D_{\text{coh}}$ , that is, more strain, defects, and dislocations, has therefore a large impact and a strong influence on the precise electronic landscape of the thin films. This assumption is further confirmed by the C60 data. Since C60 is a spherical molecule, the molecular orbitals are uniformly distributed in every spatial direction and the impact of defects on the gap state density is expected to be independent of a predominant direction.<sup>52</sup> As can be seen in Figure 7d, this is the case with an overall decrease of defect density and the gap state density following the trend of both out-of-plane defect density and the in-plane defect density. Further insight into the origin of gap states is gained by comparing the absolute values of the gap state density with the absolute value of the in-plane defect density (Figures S1 and S2). We find the gap state densities of PEN and PFP to be significantly smaller than those for [6]phenacene and C60, which correspond well to the difference in structural defect density between the former and latter. Additionally, we can conclude that a key factor governing the ELA at the substrate/organic interface is the energy gap between substrate Fermi energy and HOMO/LUMO states and the exact distribution of the density of gap states. If the energy barrier between the substrate Fermi energy and the HOMO/LUMO states is small enough, an interface dipole, due to charge transfer, can be observed. Its magnitude depends strongly on the gap state density with more charges transferred when the substrate temperature is decreased during growth.

In summary, by adjusting the density of structural defects (e.g., by temperature variation, exposition to gases, or sputtering techniques), the ELA at inorganic/organic interfaces can be controlled. This opens up new possibilities for tuning the functionality and increasing the efficiency of devices based on organic semiconductors such as organic light-emitting diodes (OLEDs) or organic solar cells.

## ■ ASSOCIATED CONTENT

### SI Supporting Information

The Supporting Information is available free of charge at <https://pubs.acs.org/doi/10.1021/acs.jpcc.1c03096>.

UPS data for a wider energy range, fitting parameters for the exponential gap state tails in Figure 2, and direct boundary length measurements from AFM images and the Williamson–Hall and mosaicity analysis (PDF)

## ■ AUTHOR INFORMATION

### Corresponding Author

Alexander Hinderhofer – Institute for Applied Physics, University of Tübingen, Tübingen 72076, Germany; [orcid.org/0000-0001-8152-6386](https://orcid.org/0000-0001-8152-6386); Email: [alexander.hinderhofer@uni-tuebingen.de](mailto:alexander.hinderhofer@uni-tuebingen.de)

### Authors

Jan Hagenlocher – Institute for Applied Physics, University of Tübingen, Tübingen 72076, Germany  
Niels Scheffczyk – Institute for Applied Physics, University of Tübingen, Tübingen 72076, Germany  
Katharina Broch – Institute for Applied Physics, University of Tübingen, Tübingen 72076, Germany; [orcid.org/0000-0002-9354-292X](https://orcid.org/0000-0002-9354-292X)

Giuliano Duva – Institute for Applied Physics, University of Tübingen, Tübingen 72076, Germany; [orcid.org/0000-0001-9492-3276](https://orcid.org/0000-0001-9492-3276)

Nadine Rußegger – Institute for Applied Physics, University of Tübingen, Tübingen 72076, Germany

Lisa Egenberger – Institute for Applied Physics, University of Tübingen, Tübingen 72076, Germany

Rupak Banerjee – Department of Physics, Indian Institute of Technology Gandhinagar, Gandhinagar 382355, India; [orcid.org/0000-0002-1189-1502](https://orcid.org/0000-0002-1189-1502)

Satoshi Kera – Department of Photo-Molecular Science, Institute for Molecular Science, Okazaki 444-8585, Japan; [orcid.org/0000-0003-0353-5863](https://orcid.org/0000-0003-0353-5863)

Frank Schreiber – Institute for Applied Physics, University of Tübingen, Tübingen 72076, Germany

Complete contact information is available at:

<https://pubs.acs.org/doi/10.1021/acs.jpcc.1c03096>

## Notes

The authors declare no competing financial interest.

## ■ ACKNOWLEDGMENTS

The authors gratefully acknowledge the Diamond Light Source (DLS) and the SOLEIL Synchrotron for providing us with beamtime and the staff from I07 (DLS) and SiXS (Soleil), particularly Jonathan Rawle (DLS) and Alina Vlad (Soleil), for their support. This work was supported by the German Research Foundation (DFG) under project HI 1927/1-1. J.H. thanks the Japan Society for the Promotion of Science (JSPS) for funding during the Summer Program in Japan. G.D. gratefully acknowledges the Carl-Zeiss-Stiftung.

## ■ REFERENCES

- (1) Opitz, A. Energy level alignment at planar organic heterojunctions: influence of contact doping and molecular orientation. *J. Phys.: Condens. Matter* **2017**, *29*, 133001.
- (2) Koch, N. Energy levels at interfaces between metals and conjugated organic molecules. *J. Phys.: Condens. Matter* **2008**, *20*, 184008.
- (3) Hinderhofer, A.; Schreiber, F. Organic organic heterostructures: concepts and applications. *ChemPhysChem* **2012**, *13*, 628–643.
- (4) Banerjee, R.; Novák, J.; Frank, C.; Lorch, C.; Hinderhofer, A.; Gerlach, A.; Schreiber, F. Evidence for kinetically limited thickness dependent phase separation in organic thin film blends. *Phys. Rev. Lett.* **2013**, *110*, 185506.
- (5) Kowarik, S.; Gerlach, A.; Hinderhofer, A.; Milita, S.; Borgatti, F.; Zontone, F.; Suzuki, T.; Biscarini, F.; Schreiber, F. Structure, morphology, and growth dynamics of perfluoro-pentacene thin films. *Phys. Status Solidi Rapid Res. Lett.* **2008**, *2*, 120–122.
- (6) Ishii, H.; Sugiyama, K.; Ito, E.; Seki, K. Energy level alignment and interfacial electronic structures at organic/metal and organic/organic interfaces. *Adv. Mater.* **1999**, *11*, 605–625.
- (7) Xie, Z.; Báldea, I.; Frisbie, C. D. Determination of Energy-Level Alignment in Molecular Tunnel Junctions by Transport and Spectroscopy: Self-Consistency for the Case of Oligophenylene Thiols and Dithiols on Ag, Au, and Pt Electrodes. *J. Am. Chem. Soc.* **2019**, *141*, 3670–3681.
- (8) Cnops, K.; Zango, G.; Genoe, J.; Heremans, P.; Martinez-Diaz, M. V.; Torres, T.; Cheyns, D. Energy level tuning of non fullerene acceptors in organic solar cells. *J. Am. Chem. Soc.* **2015**, *137*, 8991–8997.
- (9) Chen, W.; Qi, D. C.; Huang, Y. L.; Huang, H.; Wang, Y. Z.; Chen, S.; Gao, X. Y.; Wee, A. T. S. Molecular orientation dependent energy level alignment at organic organic heterojunction interfaces. *J. Phys. Chem. C* **2009**, *113*, 12832–12839.

- (10) Braun, S.; Salaneck, W. R.; Fahlman, M. Energy level alignment at organic/metal and organic/organic interfaces. *Adv. Mater.* **2009**, *21*, 1450–1472.
- (11) Salzman, I.; Duhm, S.; Heimel, G.; Oehzelt, M.; Kniprath, R.; Johnson, R. L.; Rabe, J. P.; Koch, N. Tuning the ionization energy of organic semiconductor films: the role of intramolecular polar bonds. *J. Am. Chem. Soc.* **2008**, *130*, 12870–12871.
- (12) Duhm, S.; Heimel, G.; Salzman, I.; Glowatzki, H.; Johnson, R. L.; Vollmer, A.; Rabe, J. P.; Koch, N. Orientation dependent ionization energies and interface dipoles in ordered molecular assemblies. *Nat. Mater.* **2008**, *7*, 326–332.
- (13) Chen, M.-T.; et al. Energy-level alignment at strongly coupled organic-metal interfaces. *J. Phys.: Condens. Matter* **2019**, *31*, 194002.
- (14) Wang, H.; Levchenko, S. V.; Schultz, T.; Koch, N.; Scheffler, M.; Rossi, M. Modulation of the work function by the atomic structure of strong organic electron acceptors on H-Si (111). *Adv. Electron. Mater.* **2019**, *5*, 1800891.
- (15) Yonezawa, K.; Hinderhofer, A.; Hosokai, T.; Kato, K.; Makino, R.; Schreiber, F.; Ueno, N.; Kera, S. Structural defects control the energy level alignment at organic/organic interfaces. *Adv. Mater. Interfaces* **2014**, *1*, 1400004.
- (16) Yang, J.-P.; Bussolotti, F.; Kera, S.; Ueno, N. Origin and role of gap states in organic semiconductor studied by UPS: as the nature of organic molecular crystals. *J. Phys. D: Appl. Phys.* **2017**, *50*, 423002.
- (17) Li, S.-C.; Wang, J.-g.; Jacobson, P.; Gong, X.-Q.; Selloni, A.; Diebold, U. Correlation between bonding geometry and band gap states at organic inorganic interfaces: catechol on rutile TiO<sub>2</sub> (110). *J. Am. Chem. Soc.* **2009**, *131*, 980–984.
- (18) Lange, I.; Blakesley, J. C.; Frisch, J.; Vollmer, A.; Koch, N.; Neher, D. Band bending in conjugated polymer layers. *Phys. Rev. Lett.* **2011**, *106*, 216402.
- (19) Oehzelt, M.; Akaike, K.; Koch, N.; Heimel, G. Energy level alignment at organic heterointerfaces. *Sci. Adv.* **2015**, *1*, No. e1501127.
- (20) Oehzelt, M.; Koch, N.; Heimel, G. Organic semiconductor density of states controls the energy level alignment at electrode interfaces. *Nat. Commun.* **2014**, *5*, 4174.
- (21) Beljonne, D.; Cornil, J.; Muccioli, L.; Zannoni, C.; Brédas, J.-L.; Castet, F. Electronic processes at organic organic interfaces: Insight from modeling and implications for opto electronic devices. *Chem. Mater.* **2011**, *23*, 591–609.
- (22) Bussolotti, F.; Yang, J.; Hinderhofer, A.; Huang, Y.; Chen, W.; Kera, S.; Wee, A. T. S.; Ueno, N. Origin of the energy level alignment at organic/organic interfaces: The role of structural defects. *Phys. Rev. B: Condens. Matter Mater. Phys.* **2014**, *89*, 115319.
- (23) Gmucová, K.; Nádaždy, V.; Schauer, F.; Kaiser, M.; Majková, E. Electrochemical spectroscopic methods for the fine band gap electronic structure mapping in organic semiconductors. *J. Phys. Chem. C* **2015**, *119*, 15926–15934.
- (24) Anthony, J. E.; Brooks, J. S.; Eaton, D. L.; Parkin, S. R. Functionalized pentacene: improved electronic properties from control of solid state order. *J. Am. Chem. Soc.* **2001**, *123*, 9482–9483.
- (25) Kera, S.; Ueno, N. Photoelectron spectroscopy on the charge reorganization energy and small polaron binding energy of molecular film. *J. Electron Spectrosc. Relat. Phenom.* **2015**, *204*, 2–11.
- (26) Bussolotti, F.; Yang, J.; Hiramoto, M.; Kaji, T.; Kera, S.; Ueno, N. Direct detection of density of gap states in C 60 single crystals by photoemission spectroscopy. *Phys. Rev. B: Condens. Matter Mater. Phys.* **2015**, *92*, 115102.
- (27) Salzman, I.; Heimel, G.; Oehzelt, M.; Winkler, S.; Koch, N. Molecular electrical doping of organic semiconductors: fundamental mechanisms and emerging dopant design rules. *Acc. Chem. Res.* **2016**, *49*, 370–378.
- (28) Kowarik, S.; Gerlach, A.; Schreiber, F. Organic molecular beam deposition: fundamentals, growth dynamics, and in situ studies. *J. Phys.: Condens. Matter* **2008**, *20*, 184005.
- (29) Schreiber, F. Organic molecular beam deposition: Growth studies beyond the first monolayer. *Phys. Status Solidi A* **2004**, *201*, 1037–1054.
- (30) Verlaak, S.; Rolin, C.; Heremans, P. Microscopic description of elementary growth processes and classification of structural defects in pentacene thin films. *J. Phys. Chem. B* **2007**, *111*, 139–150.
- (31) Jacobs, H. O.; Leuchtmann, P.; Homan, O. J.; Stemmer, A. Resolution and contrast in Kelvin probe force microscopy. *J. Appl. Phys.* **1998**, *84*, 1168–1173.
- (32) Collins, L.; Kilpatrick, J. I.; Weber, S. A. L.; Tselev, A.; Vlasiouk, I. V.; Ivanov, I. N.; Jesse, S.; Kalinin, S. V.; Rodriguez, B. J. Open loop Kelvin probe force microscopy with single and multi-frequency excitation. *Nanotechnology* **2013**, *24*, 475702.
- (33) Queisser, H. J.; Haller, E. E. Defects in semiconductors: some fatal, some vital. *Science* **1998**, *281*, 945–950.
- (34) Nguyen, T. P. Defect analysis in organic semiconductors. *Mater. Sci. Semicond. Process.* **2006**, *9*, 198–203.
- (35) Nguyen, T. P. Defects in organic electronic devices. *Phys. Status Solidi A* **2008**, *205*, 162–166.
- (36) Yang, Y. S.; Kim, S. H.; Lee, J.-I.; Chu, H. Y.; Do, L.-M.; Lee, H.; Oh, J.; Zyung, T.; Ryu, M. K.; Jang, M. S. Deep level defect characteristics in pentacene organic thin films. *Appl. Phys. Lett.* **2002**, *80*, 1595–1597.
- (37) Nickel, B.; Barabash, R.; Ruiz, R.; Koch, N.; Kahn, A.; Feldman, L. C.; Haglund, R. F.; Scoles, G. Dislocation arrangements in pentacene thin films. *Phys. Rev. B* **2004**, *70*, 125401.
- (38) Krug, J. Origins of scale invariance in growth processes. *Adv. Phys.* **1997**, *46*, 139–282.
- (39) Hinderhofer, A.; Hosokai, T.; Frank, C.; Novák, J.; Gerlach, A.; Schreiber, F. Templating effect for organic heterostructure film growth: Perfluoropentacene on diindenoperylene. *J. Phys. Chem. C* **2011**, *115*, 16155–16160.
- (40) Nečas, D.; Klapetek, P. Gwyddion: an open-source software for SPM data analysis. *Cent. Eur. J. Phys.* **2012**, *10*, 181–188.
- (41) Frank, C.; Novák, J.; Gerlach, A.; Ligorio, G.; Broch, K.; Hinderhofer, A.; Aufderheide, A.; Banerjee, R.; Nervo, R.; Schreiber, F. Real time X ray scattering studies on temperature dependence of perfluoropentacene thin film growth. *J. Appl. Phys.* **2013**, *114*, 043515.
- (42) Komura, N.; Goto, H.; He, X.; Mitamura, H.; Eguchi, R.; Kaji, Y.; Okamoto, H.; Sugawara, Y.; Gohda, S.; Sato, K.; et al. Characteristics of [6] phenacene thin film field-effect transistor. *Appl. Phys. Lett.* **2012**, *101*, 083301.
- (43) Hinderhofer, A.; Gerlach, A.; Broch, K.; Hosokai, T.; Yonezawa, K.; Kato, K.; Kera, S.; Ueno, N.; Schreiber, F. Geometric and electronic structure of templated C60 on diindenoperylene thin films. *J. Phys. Chem. C* **2013**, *117*, 1053–1058.
- (44) Ungár, T.; Tichy, G.; Gubicza, J.; Hellmig, R. J. Correlation between subgrains and coherently scattering domains. *Powder Diffraction* **2005**, *20*, 366–375.
- (45) Camillone, N., III; Chidsey, C. E. D.; Eisenberger, P.; Fenter, P.; Li, J.; Liang, K. S.; Liu, G. Y.; Scoles, G. Structural defects in self assembled organic monolayers via combined atomic beam and x ray diffraction. *J. Chem. Phys.* **1993**, *99*, 744–747.
- (46) Yamoah, N. K.; Koten, M. A.; Thompson, D.; Nannuri, C.; Narayan, J.; Shield, J. E.; Kumar, D. Dependence of grain size and defect density on the magnetic properties of mechanically alloyed Fe<sub>90</sub>W<sub>10</sub> powder. *J. Appl. Phys.* **2016**, *120*, 143903.
- (47) Kamei, T.; Kondo, M.; Matsuda, A. A significant reduction of impurity contents in hydrogenated microcrystalline silicon films for increased grain size and reduced defect density. *Jpn. J. Appl. Phys.* **1998**, *37*, L265.
- (48) Vázquez, H.; Flores, F.; Kahn, A. Induced density of states model for weakly-interacting organic semiconductor interfaces. *Org. Electron.* **2007**, *8*, 241–248.
- (49) Yoshida, H.; Yamada, K.; Tsutsumi, J.; Sato, N. Complete description of ionization energy and electron affinity in organic solids: Determining contributions from electronic polarization, energy band dispersion, and molecular orientation. *Phys. Rev. B: Condens. Matter Mater. Phys.* **2015**, *92*, 075145.
- (50) Yoshida, H. Low-energy inverse photoemission study on the electron affinities of fullerene derivatives for organic photovoltaic cells. *J. Phys. Chem. C* **2014**, *118*, 24377–24382.

(51) Kubozono, Y.; He, X.; Hamao, S.; Teranishi, K.; Goto, H.; Eguchi, R.; Kambe, T.; Gohda, S.; Nishihara, Y. Transistor application of phenacene molecules and their characteristics. *Eur. J. Inorg. Chem.* **2014**, *2014*, 3806–3819.

(52) Verlaak, S.; Beljonne, D.; Cheyns, D.; Rolin, C.; Linares, M.; Castet, F.; Cornil, J.; Heremans, P. Electronic structure and geminate pair energetics at organic organic interfaces: the case of pentacene/C60 heterojunctions. *Adv. Funct. Mater.* **2009**, *19*, 3809–3814.